

## **Serial passaging causes extensive positive selection in seasonal influenza A hemagglutinin**

Claire D. McWhite<sup>1,2</sup>, Austin G. Meyer<sup>1,3,4</sup>, Claus O. Wilke<sup>1,3,4</sup>

<sup>1</sup>Center for Systems and Synthetic Biology and Institute for Cellular and Molecular Biology, The University of Texas at Austin, Austin, TX 78712

<sup>2</sup>Department of Molecular Biosciences, The University of Texas at Austin, Austin, TX 78712

<sup>3</sup>Center for Computational Biology and Bioinformatics, The University of Texas at Austin, Austin, TX 78712

<sup>4</sup>Department of Integrative Biology, The University of Texas at Austin, Austin, TX 78712

Address correspondence to [wilke@austin.utexas.edu](mailto:wilke@austin.utexas.edu)

Influenza A human isolates are rarely sequenced directly. Instead, a majority of these isolates (~70% in 2015) are first subjected to serial passaging for amplification, most commonly in non-human cell culture. Here, we find that this passaging leaves distinct signals of adaptation in the viral sequences, and it confounds evolutionary analyses of the viral sequences. We find distinct patterns of adaptation to generic (MDCK) and monkey cell culture. These patterns also dominate pooled data sets not separated by passaging type. By contrast, MDCK-SIAT1 passaged sequences seem mostly (but not entirely) free of passaging adaptations. Contrary to previous studies, we find that using only internal branches of the influenza phylogenetic trees is insufficient to correct for passaging artifacts. These artifacts can only be safely avoided by excluding passaged sequences entirely from subsequent analysis. We conclude that all future influenza evolutionary analyses must appropriately control for potentially confounding effects of passaging adaptations.

## INTRODUCTION

The routine sequencing of clinical isolates has become a critical component of global seasonal influenza surveillance (World Health Organization Global influenza surveillance network, 2011). Analysis of these viral sequences informs the selection of future vaccine strains (Stöhr et al., 2012; WHO Writing Group et al., 2012), and a wide variety of computational methods have been developed to identify sites under selection or immune-escape mutations (Blackburne et al., 2008; Koelle et al., 2006; Nelson et al., 2006; Suzuki, 2008; Wolf et al., 2006), or to predict the short-term evolutionary future of influenza virus (Łuksza and Lässig, 2014; Neher et al., 2014). However, sites that appear positively selected in sequence analysis frequently do not agree with sites identified experimentally in hemagglutination inhibition assays (Meyer and Wilke, 2015; Tusche et al., 2012), and the origin of this discrepancy is unclear. Here, we argue that a major cause of this discrepancy is widespread serial passaging of influenza virus before sequencing.

Clinical isolates are generally passaged in culture to amplify viral copy number, as well as to introduce virus into a living system for testing strain features such as vaccine response, antiviral response, and replication efficiency (Kumar and Henrickson, 2012; World Health Organization Global influenza surveillance network, 2011). A variety of culture systems are used for virus amplification. Cell cultures derived from Madin-Darby canine kidney (MDCK) cells are by far the most widely used system, with the majority of sequences in influenza repositories deriving from virus that has been passaged through an MDCK cell culture (Balish et al., 2005; Bogner et al., 2006). Influenza virus may also be passaged through monkey kidney (RhMK or TMK) cell culture or injected directly into egg amniotes. Alternatively, complete influenza genomes can be obtained from PCR-amplified influenza samples without intermediate passaging (Katz et al., 1990; Lee et al., 2013a).

Several experiments have demonstrated that influenza hemagglutinin (HA) accumulates mutations following rounds of serial passaging in both cell (Ilyushina et al., 2012; Lee et al., 2013b; Wyde et al., 1977) and egg culture (Robertson et al., 1993). The decreased number of mutations in MDCK-based cell culture is the main argument for use of this system over egg amniotes in vaccine production (Katz and Webster, 1989), with MDCK cells expressing human SIAT1 having the highest fidelity to the original sequence and reduced host adaptation (Hamamoto et al., 2013). Viral adaptations to eggs have recently been linked to reduced vaccine efficacy (Skowronski et al., 2014; Xie et al., 2015) and were implicated as potentially contributing to reduced efficacy of 2014-2015 seasonal H3N2 influenza vaccination in the World Health Organization's recommendations for 2015-2016 vaccine strains (The World Health Organization, 2015). As the majority of influenza vaccines worldwide are produced in eggs, vaccine strain selection is limited to virus with the ability to replicate rapidly in this system (World Health Organization Global influenza surveillance network, 2011).

Although egg-passaged sequences are increasingly excluded from influenza phylogenetic analysis (see e.g. the NextFlu tracker (Neher and Bedford, 2015)), due to the known high host-specific substitution rates, cell culture is generally not thought to be sufficiently selective to produce a discernable evolutionary signal. One of few existing evolutionary analyses of passaging effects on influenza (Bush et al., 2000) demonstrated that passaging causes no major changes in clade structure between egg and cell passaged viruses. Moreover, several studies have recommended the use of internal branches in the phylogenetic tree to reduce passaging effects in evolutionary analysis of Influenza A (Bush et al., 2001; Suzuki, 2006). Another study discovered egg culture to be the cause of misidentification of several sites under positive selection in Influenza B (Gatherer, 2010), but this study was limited to comparing egg-cultured to cell-cultured virus. As the availability of unpassaged influenza sequences has dramatically increased over the past ten years, we can now perform a direct comparison of passaged to circulating virus.

Here, we compare patterns of adaptation in North American seasonal H3N2 influenza HA sequences derived from passaged and unpassaged virus. We divide viral sequences by their passaging history, distinguishing between unpassaged clinical samples, egg amniotes, RhMK (monkey) cell culture, and generic/MDCK-based cell culture. For the latter, we also distinguish between virus passaged in MDCK-SIAT1 cell culture (SIAT1) and in unmodified MDCK or unspecified cell culture (non-SIAT1). We find clear signals of adaptation to the various passaging conditions. These signals are strongly present in the tip branches of the phylogenetic trees but can also be detected in internal branches. Finally, we demonstrate that the identification of antigenic escape sites from sequence data has been confounded by passaging adaptations, and that the exclusion of passaged sequences allows us to use sequence and structural data to highlight regions involved in antigenic escape.

## RESULTS

Most influenza-virus samples collected from patients are first serially passaged through one or more culturing systems, prior to PCR amplification and sequencing (Figure 1A). Reconstructed trees of influenza evolution contain a mixture of passage histories at their tips (Figure 1B). During serial passaging, influenza genomes accumulate adaptive mutations, and the effect of these mutations on evolutionary analyses of influenza sequences is not well understood.

### **Sitewise evolutionary rate patterns differ between passage groups**

To quantify any evolutionary signal that may be introduced by passaging, we assembled, from the GISAID database (Bogner et al., 2006), a set of North American human influenza H3N2 hemagglutinin sequences collected between 2005 and 2015. We initially sorted these sequences into groups by their passage history: (1) unpassaged, (2) egg-passaged, (3) generic cell-passaged, and (4) monkey cell-passaged (Table 1). To assess evolutionary variation at individual sites, we calculated

site-specific  $dN/dS$  (Echave et al., 2016), using Single Likelihood Ancestor Counting (SLAC). Specifically, we calculated one-rate  $dN/dS$  estimates, i.e., site-specific  $dN$  values normalized by a global  $dS$  value (see Methods for details). In addition to considering groups of sequences with specific passage histories, we also calculated  $dN/dS$  values by pooling all sequences into one combined analysis. This pooled group corresponds to a typical influenza evolutionary analysis in which passage history has not been accounted for.

We first correlated the sitewise  $dN/dS$  values we obtained for virus sequences derived from different passage histories. If passage history did not matter, then the  $dN/dS$  values obtained from different sources should correlate strongly with each other, with  $r$  approaching 1. Instead, we found that correlation coefficients ranged from 0.68 to 0.88, depending on which specific comparison we made (Figure 2A). (In this analysis, and throughout this work, we down-sampled alignments to the smallest number of sequences available for any of the conditions compared, to keep the samples as comparable as possible overall. The analysis of Figure 2 used  $n = 917$  randomly drawn sequences for each condition.) Unpassed  $dN/dS$  correlated more strongly with cell and pooled  $dN/dS$  (correlations of 0.77 and 0.79, respectively) than with monkey-cell  $dN/dS$  (0.68). Note that the  $dN/dS$  values from the pooled group, which corresponds to a typical data set used in a phylogenetic analysis of influenza, more closely correlated with the  $dN/dS$  values from the generic cell group ( $r = 0.87$ ) than from the unpassed group ( $r = 0.79$ ). Egg-derived sequences were excluded from this analysis due to low sequence numbers ( $n = 79$ ), however evolutionary rates from this condition correlated particularly poorly with those of random draws of 79 unpassed sequences (Supplementary Figure 1). This result is consistent with the conclusions of (Bush et al., 2000), (Suzuki, 2006), and (Gatherer, 2010) that egg-derived sequences show specific adaptations not found otherwise in influenza sequences.

Because the common ancestor of any two passaged influenza viruses is a virus that replicated in humans, we would expect that any adaptations introduced during passaging should not extend into the internal branches of a reconstructed tree. Therefore, we additionally subdivided phylogenetic trees into internal branches and tip branches, and calculated site-specific  $dN/dS$  values separately for these two sets of branches. In fact, (Bush et al., 2000) had recommended the use of internal branches to reduce variation seen between egg and non-egg passaged virus. As expected, we found that when  $dN/dS$  calculations were restricted to the internal branches, the correlations between the passage groups overall increased (Figure 2B), even though distinct differences between the passage groups remained. Conversely, when only considering tip branches, correlations among most groups were relatively low (Figure 2C), with the exception of cell-passaged sequences compared to the pooled sequences. This finding emphasizes once again that the pooled sample is most similar to the cell-passaged sample. We conclude that different passaging histories leave distinct, evolutionary signatures of adaptation to the passaging environment.

To further investigate the apparent discrepancies between  $dN/dS$  derived from unpassaged sequences, monkey-cell passaged sequences, cell-passaged sequences, and the pooled set, we compared the magnitude of the site-wise rates (Figure 2D). Cell-passaged and pooled sequences had, on average, significantly inflated  $dN/dS$  values compared to unpassaged and monkey-cell-passaged sequences in the full phylogenetic tree (paired  $t$  test,  $P = 1.5 \times 10^{-05}$  and  $P = 9.1 \times 10^{-05}$ , respectively) and along tip branches (paired  $t$  test,  $P = 1.8 \times 10^{-06}$  and  $P = 6.3 \times 10^{-05}$ , respectively). By contrast, there were no significant differences between cell-passaged and pooled sequences in all three cases (paired  $t$  test,  $P = 0.26$ ,  $P = 0.24$ , and  $P = 0.26$ , respectively, for the full tree, internal branches, and tip branches).  $dN/dS$  values were generally more similar along internal branches, however a significant difference of  $dN/dS$  from cell-passaged and pooled sequences relative to monkey-cell-passaged sequences remained. These results demonstrate that both cell-passaged and pooled sequences show artificially inflated  $dN/dS$  values compared to unpassaged sequences.

In aggregate, these results show that while both generic-cell-passaged sequences and monkey-cell-passaged sequences yield different sitewise  $dN/dS$  patterns relative to unpassaged sequences (Fig. 2A-C), cell passaging additionally creates inflated  $dN/dS$  values (Fig. 2D), indicating positive adaptation to the passaging condition. At the same time,  $dN/dS$  values derived from monkey-cell-passaged sequences are the least similar to  $dN/dS$  from unpassaged sequences (Fig. 2A-C). The pooled group of sequences, which corresponds to a typical data set used in evolutionary analyses of influenza virus, describes evolutionary rates of specifically cell passaged virus and poorly matches evolutionary rates of circulating influenza virus.

### **Adaptations to cell and monkey-cell passage display characteristic patterns of site variation**

We next asked whether adaptations to passage history were located in specific regions of the HA protein. To address this question, we employed the geometric model of HA evolution we recently introduced (Meyer and Wilke, 2015). For H3N2 HA, this model explains over 30% of the variation in  $dN/dS$  using two simple physical measures, the relative solvent accessibility (RSA) of individual residues in the structure (Tien et al., 2013) and the inverse linear distance in 3D space from each residue to protein site 224 in the hemagglutinin monomer. Notably, the geometric model was previously applied to a pooled sequence set including sequences of various passaging histories. To what extent it carries over to sequences with specific passaging histories is not known.

We first considered the correlation between  $dN/dS$  and RSA (Figure 3A). We found that for all passage groups,  $R^2$  values ranged from 0.10 to 0.16 in the full tree, consistent with our earlier work (Meyer and Wilke, 2015). The high congruence among  $R^2$  values for internal branches and all branches suggests that RSA imposes a pervasive selection pressure on HA, independent of passaging adaptations. Thus, RSA represents a useful



structural measure of a persistent effect of  $dN/dS$  with stronger correlations in the full tree and internal branches than in tip branches.

Next we considered the correlation between  $dN/dS$  and the inverse distance to site 224 (Figure 3B). In contrast to RSA, correlations here were systematically higher in tip branches, suggesting a recent adaptive signal. We found virtually no correlation for unpassaged sequences, while a low correlation existed for monkey-cell cultured sequences and a higher correlation for cell-passaged and pooled sequences. Correlations from pooled sequences mirrored cell culture correlations and persisted through internal branches. Thus, the correlation of  $dN/dS$  with the inverse distance to site 224 seems to be primarily an artifact of cell passage, even though its effect can be seen along internal branches as well. As the majority of the available HA sequences are cell-derived, this cell-specific signal dominates the pooled data set. Further, this cell-specific signal is partially attenuated along internal branches and amplified along tip branches, as we would expect from a signal caused by recent host-specific adaptation. Even though this signal is a true predictor of influenza evolutionary rates for virus grown in cell culture, it does not transfer to unpassaged sequences and therefore has no relevance for the circulating virus. This finding serves as a strong demonstration of passage history as a confounder in evolutionary analysis of hemagglutinin evolution, not just for egg passage as previously demonstrated, but also for cell and monkey-cell passage.

Surprisingly, the correlation we found here between  $dN/dS$  and inverse distance to site 224 for pooled sequences ( $R^2 = 0.067$ ) was less than half of the value reported by (Meyer and Wilke, 2015) (Fig. 3B). However, using a dataset of sequences more temporally matched to that paper's dataset (2005–2014 instead of 2005–2015), we recovered the previously seen higher correlation. This finding suggests that there is some feature in the additional 2015 sequences that changes the pooled dataset's relationship with inverse distance to site 224. In 2015, unpassaged and SIAT1 sequenced each doubled in number compared to in 2014, while the number of non-SIAT1 cell cultured sequences dropped dramatically (Table 2). Therefore, we next investigated whether the drop in correlation from 2014 to 2015 could be attributed to the recent reduction in cell culture using non-SIAT1 cells.

### **There is little signal of adaptation to passage in SIAT1 cells**

In the preceding analyses, we lumped all cell cultures except monkey cells into the same category. However, there are more subtle distinctions in cell passaging systems, and they can exert differential selective pressures on human adapted virus (Hamamoto et al., 2013; Oh et al., 2008). As our generic cell culture group was composed of a mixture of wild type MDCK, SIAT1, and unspecified cell cultures, we next investigated whether any one culture type was the source of the high cell-culture signal in Figure 3B.

The SIAT1 cell system, which overexpresses human-like 6-linked sialic acids over native 3-linked sialic acids (Matrosovich et al., 2003), is currently the dominant system for serial passaging of influenza virus. Approximately half of the 2015 influenza sequences currently available from GISAID derive from serial passaging through SIAT1 cells. Experimental analysis of SIAT1 demonstrates improved sequence fidelity and reduced positive selection over unmodified MDCK cell culture (Hamamoto et al., 2013; Oh et al., 2008). We sought to determine if the apparently cell-culture-specific correlation of site-wise evolutionary rates and inverse distance to site 224 extended to SIAT1 cell culture. To compare cell-culture varieties, we created sample-size matched groups of non-SIAT1 cell culture, SIAT1 cell culture, and unpassaged sequences collected between 2005 and 2015 ( $n = 1046$ ), excluding sequences that had been passaged through both a non-SIAT1 and a SIAT1 cell culture.

All groups showed similar correlations between  $dN/dS$  and RSA, regardless of whether  $dN/dS$  was calculated for the entire tree, for internal branches only, or for tip branches only (Figure 4A). By contrast, inverse distance to site 224 uniquely correlated with  $dN/dS$  from non-SIAT1-cultured virus (Figure 4B). This effect was the strongest along tip branches ( $R^2 = 0.139$ ), but it was almost as strong along the entire tree ( $R^2 = 0.129$ ). The correlation was reduced, though still significant, among internal branches ( $R^2 = 0.075$ ). Thus, we conclude that the correlation between  $dN/dS$  and the inverse distance to site 224 (Meyer and Wilke, 2015) represents a unique signal of adaptation to passaging in non-SIAT1 cells. In our previous analysis (Meyer and Wilke, 2015), a non-SIAT1-specific signal completely dominated our evolutionary rate models, due to use of a standard, pooled data set mainly composed of sequences passaged in non-SIAT1 cells. In our new analysis (Figure 3B), the high correlation of non-SIAT1 cell  $dN/dS$  with inverse distance to site 224 is suppressed in the pooled condition, because the number of unpassaged and SIAT1-passaged sequences grew substantially in 2015. This difference in sample composition explains the lower than expected correlations in Figure 3B for pooled  $dN/dS$ .

When considering all branches in the phylogenetic tree, we found that  $dN/dS$  values were significantly inflated in sequences passaged in non-SIAT1 cells compared to both unpassaged and SIAT1-passaged sequences (paired  $t$  test,  $P = 5.05 \times 10^{-6}$  and  $P = 6.94 \times 10^{-8}$ , respectively, Figure 4C), whereas unpassaged and SIAT1-passaged sequences showed no significant increase (Figure 4C). Unpassaged and non-SIAT1-passaged sequences showed significant differences along internal branches (paired  $t$  test,  $P = 0.036$ ) and tip branches as well (paired  $t$  test,  $P = 2.03 \times 10^{-6}$ , Figure 4C). Thus, virus amplified in non-SIAT1 cell culture measurably adapts to this non-human host, and these adaptations can significantly confound downstream evolutionary analyses.

As these three conditions are somewhat temporally separated (most non-SIAT1 cell culture sequences are pre-2015, and most unpassaged and SIAT1 culture sequences are post-2014), we controlled for season-to-season variation by drawing 249 sequences



from each group from 2014. First, we again considered site-wise  $dN/dS$  correlations among passaging groups, and we found that overall, unpassaged and SIAT1-passaged sequences appeared the most similar (Supplementary Figure 2A–C). However, both SIAT1 and non-SIAT1 showed  $dN/dS$  values that were inflated over  $dN/dS$  in unpassaged sequences when considering the full tree (paired  $t$  test,  $P = 0.029$  and  $P = 0.0005$ , respectively, Supplementary Figure 2D), although only non-SIAT1  $dN/dS$  was significantly inflated in tip branches (paired  $t$  test,  $P = 0.0008$ , Supplementary Figure 2D). (No significant difference was seen along internal branches.) Notably, in this more controlled comparison of SIAT1 cell culture to unpassaged sequences from the same year, we observed a significant difference in  $dN/dS$  between these conditions, suggesting that at least minor passaging artifacts remain after SIAT1 passaging.

### **Evolutionary variation in sequences from unpassaged virus predicts regions involved in antigenic escape**

The preceding results might suggest that the inverse distance metric we previously proposed (Meyer and Wilke, 2015) only captures effects of adaptation to non-SIAT1 cell culture. However, this is not necessarily the case. Importantly, inverse distance needs to be calculated relative to a specific reference point. We previously used site 224 as the reference point because it yielded the highest correlation for the data set we analyzed then. For a different data set, one that doesn't carry the signal of adaptation to non-SIAT1 cell culture, a different reference point may be more appropriate.

We thus repeated the analysis of (Meyer and Wilke, 2015) for a size matched sample of 1703 sequences from both non-SIAT1 cell passaged and unpassaged virus collected between 2005 and 2015 (Figure 5). In brief, for each possible reference site in the hemagglutinin structure, we measured the inverse distance in 3D space from that site to every other site in the structure. We then correlated the inverse distances with the  $dN/dS$  values at each site, resulting in one correlation coefficient per reference site. Finally, we mapped these correlation coefficients onto the HA structure, coloring each reference site by its associated correlation coefficient. If inverse distances measured from a particular reference amino acid have higher correlation with the sitewise  $dN/dS$  values, then this reference site will appear highlighted on the structure.

For non-SIAT1-passaged virus, this analysis recovered the finding of (Meyer and Wilke, 2015) that the loop containing site 224 appeared strongly highlighted (Figure 5A). However, this signal was entirely absent in unpassaged virus (Figure 5B), with no sites in that loop working well as a reference point. These results suggest that this loop is specifically involved in adaptation of hemagglutinin to non-SIAT1 cell culture, explaining the non-SIAT1-specific signal shown in Figure 4A. Thus, the inverse distance metric is useful for differentiating regions of selection particular to different experimental groups.

(Meyer and Wilke, 2015) had concluded that sites under positive selection differed from sites involved in immune escape. Here, we have found that the origin of this positive

selection is adaptation to the non-human passaging host, not immune escape in or adaptation to humans. Therefore, we next asked what residual patterns of positive selection remained once the adaptation to non-SIAT1 cells was removed. Even though site-wise correlations are relatively low for unpassaged virus compared to the ones observed for non-SIAT1-passaged virus, we could still recover relevant patterns of HA adaptation after rescaling our coloring. In particular, we found that sites opposite to the loop containing site 224 lit up in our analysis of unpassaged sequences (Figure 6A). Sites in this region are known to be involved in antigenic escape. In fact, many of the highlighted regions contain experimentally determined antigenic sites (Koel et al., 2013) and/or the sites determined to be responsible for the antigenic shift in the 2014/2015 seasonal flu (Chambers et al., 2015) (Table 2). We found a similar pattern of concordance with antigenic sites when mapping  $dN/dS$  values directly onto the structure (Figure 6B). The inverse-distance correlations, however, performed better at identifying antigenic sites than did raw  $dN/dS$  values. When considering the 90<sup>th</sup> percentile (top 10% highest scored sites) by either metric, the inverse-distance correlations recovered 7 of 8 sites while  $dN/dS$  alone recovered only 2 of 8 sites (Table 2).

## DISCUSSION

We have found that serial passaging of influenza virus introduces a measurable signal of adaptation into the evolutionary analysis of natural influenza sequences. There are unique, characteristic patterns of adaptation to egg passage, monkey cell passage, and non-SIAT1 cell passage. Monkey cell-derived sequences show different molecule-wide evolutionary rate patterns, even though they show no  $dN/dS$  inflation when compared with unpassaged sequences. Non-SIAT1 cell-derived sequences instead display both  $dN/dS$  inflation and a hotspot of positive selection in a loop underneath the sialic-acid binding region. This hotspot has been previously noted (Meyer and Wilke, 2015) but no explanation for its origin was available. Further, we have found that virus passaged in SIAT1 cells seems to accumulate only minor passaging artifacts. Throughout our analyses, we have found limited utility to subdividing phylogenetic trees into internal and terminal branches. While signals of passage adaptation are consistently elevated along terminal branches and attenuated along internal branches, evolutionary rates along internal branches remain confounded by passaging artifacts. Finally, we could accurately recover the experimentally determined antigenic regions of hemagglutinin from evolutionary-rate analysis by using a data set consisting of only unpassaged viral sequences.

Previous studies (Bush et al., 2001; Suzuki, 2006) have suggested the use of internal branches to alleviate passage adaptations. However, we have found here that this strategy is insufficient, because the evolutionary signal of passage adaptations can often be detected along internal branches. This finding seems counterintuitive, as internal nodes should exclusively represent human-adapted virus. We suggest that passaging adaptations in internal branches may be caused by convergent evolution; if different clinical isolates converge onto the same adaptive mutations under passaging,

then these mutations may incorrectly be placed along internal branches under phylogenetic tree reconstruction. Additionally, although the use of only internal branches removes some differences between the passage groups, the exclusion of terminal sequences can obscure recent natural adaptations and thus obscure actual sites under positive selection. Therefore, analysis of internal branches is not only insufficient for eliminating artifacts from passaging adaptations but also suboptimal for detecting positive selection in seasonal H3N2 influenza.

The safest route to avoid passaging artifacts is to limit sequence data sets to only unpassaged virus, although this approach limits sequence numbers. The human-like 6-linked sialic acids in SIAT1 (Matrosovich et al., 2003) greatly reduce observed cell culture-specific adaptations, particularly in the loop of hemagglutinin which contains site 224. This lack of selection concords with multiple experiments finding low levels of adaptation in this cell line (Hamamoto et al., 2013; Oh et al., 2008). As our analysis only detected minor differences between unpassaged and SIAT1 passaged virus, we posit that this passage condition is an acceptable substitute for unpassaged clinical samples. Even so, our findings do not preclude the existence of SIAT1-specific adaptations that may confound specific analyses.

Although the majority of the sequences from the year 2015 are SIAT1-passaged or unpassaged, several hundred sequences from that year derive from monkey cell culture. The use of monkey cell culture has surged in 2014 and 2015 compared to previous years. We recommend that these recently collected sequences be excluded from influenza rate analysis, in favor of the majority of unpassaged and SIAT1-passaged sequences. As passaging is a useful and cost effective method for amplification of clinically collected virus, unpassaged viral sequences are unlikely to completely dominate influenza sequence databases in the near future. However, new human epithelial cell culture systems for influenza passaging, as in (Ilyushina et al., 2012), could soon provide an ideal system that both amplifies virus and protects it from non-human selective pressures.

Passage history should routinely be considered as a potential confounding variable in future analyses of influenza evolutionary rates. Future studies should be checked against unpassaged samples to ensure that conclusions are not based on adaptation to non-human hosts. We recommend the exclusion of viral sequences which derive from serial passage in egg amniotes, monkey kidney cell culture, and any unspecified cell culture. Prior work that did not consider passaging history may likely have been confounded by passaging adaptations. In particular, we suggest that the evolutionary markers of influenza virus determined by (Belanov et al., 2015) be reevaluated to ensure these sites are not artifacts of viral passaging. Similarly, many of the earlier studies performing site-specific evolutionary analysis of HA, such as (Bush et al., 1999; Meyer and Wilke, 2015, 2013; Pan and Deem, 2011; Shih et al., 2007; Suzuki, 2008, 2006; Tusche et al., 2012), likely contain some conclusions that can be traced back to

passaging artifacts. Additionally, even though passage artifacts do not appear to be sufficiently strong to affect clade-structure reconstruction (Bush et al., 2000), they do have the potential to cause artificially long branch lengths, due to *dN/dS* inflation, or misplaced branches, due to convergent evolution under passaging. Thus, future phylogenetic predictive models of influenza fitness and antigenicity, as in (Łuksza and Lässig, 2014), (Neher et al., 2014), and (Bedford et al., 2014), should too be checked for the presence of passage-related signals. Finally, while it is beyond the scope of this work to investigate passage history effects in other viruses, we suspect that passage-derived artifacts could be a factor in their phylogenetic analyses as well. The use of data sets free of passage adaptations will likely bring computational predictions of influenza positive selection more in line with corresponding experimental results.

Sequences without passage annotations are inadequate for reliable evolutionary analysis of influenza virus. Yet, passage annotations are often completely missing from strain information, and, when present, are often inconsistent; there is currently no standardized language to represent number and type of serial passage. We note, however, that passage annotations from the 2015 season are greatly improved when compared to previous seasons. Several major influenza repositories, including the Influenza Research Database (Squires et al., 2012) and the NCBI Influenza Virus Resource (Bao et al., 2008), do not provide any passaging annotations at all. Additionally, passage history is not required for new sequence submissions to the NCBI Genbank (Benson et al., 2012). The EpiFlu database maintained by the Global Initiative for Sharing Avian Influenza Data (GISAID) (Bogner et al., 2006) and OpenFluDB (Liechti et al., 2010), however, stand apart by providing passage history annotations for the majority of their sequences. Of these, only the OpenFluDB repository allows filtering of sequences by passage history during data download. Our results demonstrate the strength of passaging artifacts in evolutionary analysis of influenza. The lack of a universal standard for annotation of viral passage histories and a universal standard for serial passage experimental conditions complicate the analysis and mitigation of passaging effects.

## **METHODS**

### **Influenza sequence data**

Non-laboratory strain H3N2 hemagglutinin (HA) sequences collected in North America were downloaded from The Global Initiative for Sharing Avian Influenza Data (GISAID) (Bogner et al., 2006) for the 1968–2015 influenza seasons. Non-complete HA sequences were excluded. Sequences were trimmed to open reading frames, filtered to remove redundancies, and aligned by translation-alignment-back-translation and MAFFT (Kato and Standley, 2013). Sequence headers of FASTA files were standardized into an uppercase text format with non-alphanumeric characters replaced by underscores. As H3N2 strains have experienced no persistent insertion or deletion events, we deleted sequences which introduced gaps to the alignment. To ascertain overall data quality, we built a phylogenetic tree of the entire sequence set (using

FastTree 2.0 (Price et al., 2010)) and checked for any abnormal clades or other unexpected tree features. We found one abnormal clade of approximately 20 sequences with an exceptionally long branch length ( $> 0.01$ ) and removed the sequences in that clade from further analysis. Our final data set consisted of 6873 sequences from 2005-2015 as well as an outgroup of 45 sequences from 1968–1977 (not considered for further analysis). We did not consider sequences collected from 1978-2004.

### **Identification of passage history and evolutionary-rate calculations**

We divided sequences into groups by their passage history annotation and collection year, determining passage history by parsing with regular expressions for key words in FASTA headers (Table 1). We classified 1133 sequences with indeterminate or missing passage histories, or passage through multiple categories of hosts (i.e. both egg and cell), as “other”. The final data sets for individual passage groups contained between 79 and 3041 sequences (Table 1).

We next constructed phylogenetic trees for each passage group as well as one tree for a pooled data set combining all individual passage groups and other sequences. All phylogenetic trees were constructed using FastTree 2.0 (Price et al., 2010). We calculated site-specific  $dN/dS$  values using a one-rate SLAC (Single-Likelihood Ancestor Counting) model implemented in HyPhy (Pond et al., 2005). One rate models, which fit a site-specific  $dN$  and a global  $dS$ , yield more accurate estimates than two-rate models and hence are preferred (Spielman et al., 2015). Among different one-rate, site-specific models, SLAC performs nearly identical to other approaches, and it was chosen here due to its speed and ease of extracting  $dN/dS$  estimates along internal and tip branches. To obtain branch-specific estimates, we extracted the  $dN/dS$  values calculated by the SLAC algorithm at internal and tip branches.

We chose sequences from 2005-2015 as our sample set due the low number of available sequences prior to this period. As  $dN/dS$  estimates can be confounded by sample size (Spielman et al., 2015), we sought to limit this effect by down-sampling each experimental set to match the number of sequences in the smallest group being considered in a particular analysis (Table 1). To reduce season-to-season variation in the comparison of unpassaged, SIAT1, and non-SIAT1 cell culture, we performed one analysis with sequences from only 2014, which is the year that maximizes sequences available from all three conditions ( $n = 249$  each).

### **Geometric analysis of $dN/dS$ distributions**

For each site  $i$  in HA, we computed the correlation of  $dN/dS$  at every site  $j \neq i$  with the inverse Euclidian distance between  $j$  and  $i$  in the 3D crystal structure of the protein. This method is discussed in detail in (Meyer and Wilke, 2015). This correlation is then color-mapped onto the reference site. Sites spatially closest to positively selected regions in the protein have the highest correlation in this analysis. Thus, this approach allows us to



visualize regions of increased positive selection. We processed the HA PDB structure as discussed in (Meyer and Wilke, 2015), and we provide a renumbered and formatted H3N2 structure derived from PDB ID 2YP7 (Lin et al., 2012) with our data analysis code (see below).

### **Statistical analysis and data availability**

Raw influenza sequences used in this analysis are available for download from GISAID (<http://gisaid.org>) using the parameters “North America”, “H3N2”, “1976 – 2015”. Acknowledgements for sequences used in this study are available in Supplementary File 1. The complete, processed data set used in our statistical analysis is available in Supplementary Dataset 6, including protein and gene numbering, computed evolutionary rates, relative solvent accessibility for the hemagglutinin trimer, and sitewise distance to protein site 224. Relative solvent accessibility of the hemagglutinin trimer was taken from (Meyer and Wilke, 2015). Site-wise distances between all amino acids in the HA structure PDBID:2YP7 were recalculated as in (Meyer and Wilke, 2015). Statistical analysis was performed using R (Ihaka and Gentleman, 1996), and all graph figures drawn with the R package ggplot2 (Wickham, 2009). Throughout this work, \* denotes a significance of  $0.01 \leq P < 0.05$ , \*\* denotes a significance of  $0.01 \leq P < 0.05$ , and \*\*\* denotes a significance of  $P < 0.001$ .

Linear models between sitewise  $dN/dS$  and RSA or inverse distance were fit using the `lm()` function in R. Correlations were calculated using the R function `cor()` and significance determined using `cor.test()`.

Our entire analysis pipeline, instructions for running analyses and raw data (except initial sequence data per the GISAID user agreement) are available at the following Github project repository:

[https://github.com/wikelab/influenza\\_H3N2\\_passaging](https://github.com/wikelab/influenza_H3N2_passaging).

### **AUTHOR CONTRIBUTIONS**

Conceived and designed the experiments: CDM COW. Wrote scripts and analytic tools: CDM AGM. Performed the experiments: CDM. Analyzed the data: CDM COW. Wrote the paper: CDM COW.

### **ACKNOWLEDGEMENTS**

We would like to thank Sebastian Maurer-Stroh for help with interpreting passaging annotations in GISAID. This work was supported in part by NIH grant no. R01 GM088344, DTRA grant no. HDTRA1-12-C-0007, and NSF Cooperative agreement no. DBI-0939454 (BEACON Center). The funders had no role in study design, data collection and analysis, decision to publish, or preparation of the manuscript.



## REFERENCES

- Balish, A.L., Katz, J.M., Klimov, A.I., 2005. Influenza: Propagation, Quantification, and Storage, in: *Current Protocols in Microbiology*. John Wiley & Sons, Inc.
- Bao, Y., Bolotov, P., Dernovoy, D., Kiryutin, B., Zaslavsky, L., Tatusova, T., Ostell, J., Lipman, D., 2008. The Influenza Virus Resource at the National Center for Biotechnology Information. *J. Virol.* 82, 596–601. doi:10.1128/JVI.02005-07
- Bedford, T., Suchard, M.A., Lemey, P., Dudas, G., Gregory, V., Hay, A.J., McCauley, J.W., Russell, C.A., Smith, D.J., Rambaut, A., 2014. Integrating influenza antigenic dynamics with molecular evolution. *eLife* 3, e01914. doi:10.7554/eLife.01914
- Belanov, S.S., Bychkov, D., Benner, C., Ripatti, S., Ojala, T., Kankainen, M., Lee, H.K., Tang, J.W.-T., Kainov, D.E., 2015. Genome-wide analysis of evolutionary markers of human influenza A(H1N1)pdm09 and A(H3N2) viruses may guide selection of vaccine strain candidates. *Genome Biol. Evol.* evv240. doi:10.1093/gbe/evv240
- Benson, D.A., Karsch-Mizrachi, I., Clark, K., Lipman, D.J., Ostell, J., Sayers, E.W., 2012. GenBank. *Nucleic Acids Res.* 40, D48–D53. doi:10.1093/nar/gkr1202
- Blackburne, B.P., Hay, A.J., Goldstein, R.A., 2008. Changing Selective Pressure during Antigenic Changes in Human Influenza H3. *PLoS Pathog* 4, e1000058. doi:10.1371/journal.ppat.1000058
- Bogner, P., Capua, I., Lipman, D.J., Cox, N.J., others, 2006. A global initiative on sharing avian flu data. *Nature* 442, 981–981. doi:10.1038/442981a
- Bush, R.M., Fitch, W.M., Bender, C.A., Cox, N.J., 1999. Positive selection on the H3 hemagglutinin gene of human influenza virus A. *Mol. Biol. Evol.* 16, 1457–1465.
- Bush, R.M., Fitch, W.M., Smith, C.B., Cox, N.J., 2001. Predicting influenza evolution: the impact of terminal and egg-adapted mutations. *Int. Congr. Ser.* 1219, 147–153. doi:10.1016/S0531-5131(01)00643-4
- Bush, R.M., Smith, C.B., Cox, N.J., Fitch, W.M., 2000. Effects of passage history and sampling bias on phylogenetic reconstruction of human influenza A evolution. *Proc. Natl. Acad. Sci.* 97, 6974–6980. doi:10.1073/pnas.97.13.6974
- Chambers, B.S., Parkhouse, K., Ross, T.M., Alby, K., Hensley, S.E., 2015. Identification of Hemagglutinin Residues Responsible for H3N2 Antigenic Drift during the 2014–2015 Influenza Season. *Cell Rep.* 12, 1–6. doi:10.1016/j.celrep.2015.06.005
- Echave, J., Spielman, S.J., Wilke, C.O., 2016. Causes of evolutionary rate variation among protein sites. *Nat. Rev. Genet.* doi:10.1038/nrg.2015.18
- Gatherer, D., 2010. Passage in egg culture is a major cause of apparent positive selection in influenza B hemagglutinin. *J. Med. Virol.* 82, 123–127. doi:10.1002/jmv.21648
- Hamamoto, I., Takaku, H., Tashiro, M., Yamamoto, N., 2013. High Yield Production of Influenza Virus in Madin Darby Canine Kidney (MDCK) Cells with Stable Knockdown of IRF7. *PLoS ONE* 8, e59892. doi:10.1371/journal.pone.0059892
- Ihaka, R., Gentleman, R., 1996. R: A Language for Data Analysis and Graphics. *J. Comput. Graph. Stat.* 5, 299–314. doi:10.2307/1390807
- Ilyushina, N.A., Ikizler, M.R., Kawaoka, Y., Rudenko, L.G., Treanor, J.J., Subbarao, K., Wright, P.F., 2012. Comparative study of influenza virus replication in MDCK cells and in primary cells derived from adenoids and airway epithelium. *J. Virol.* 86, 11725–11734. doi:10.1128/JVI.01477-12
- Katoh, K., Standley, D.M., 2013. MAFFT Multiple Sequence Alignment Software Version 7: Improvements in Performance and Usability. *Mol. Biol. Evol.* 30, 772–780. doi:10.1093/molbev/mst010

- Katz, J.M., Wang, M., Webster, R.G., 1990. Direct sequencing of the HA gene of influenza (H3N2) virus in original clinical samples reveals sequence identity with mammalian cell-grown virus. *J. Virol.* 64, 1808–1811.
- Katz, J.M., Webster, R.G., 1989. Efficacy of Inactivated Influenza A Virus (H3N2) Vaccines Grown in Mammalian Cells or Embryonated Eggs. *J. Infect. Dis.* 160, 191–198. doi:10.1093/infdis/160.2.191
- Koel, B.F., Burke, D.F., Bestebroer, T.M., van der Vliet, S., Zondag, G.C.M., Vervaet, G., Skepner, E., Lewis, N.S., Spronken, M.I.J., Russell, C.A., Eropkin, M.Y., Hurt, A.C., Barr, I.G., de Jong, J.C., Rimmelzwaan, G.F., Osterhaus, A.D.M.E., Fouchier, R.A.M., Smith, D.J., 2013. Substitutions near the receptor binding site determine major antigenic change during influenza virus evolution. *Science* 342, 976–979. doi:10.1126/science.1244730
- Koelle, K., Cobey, S., Grenfell, B., Pascual, M., 2006. Epochal evolution shapes the phylodynamics of interpandemic influenza A (H3N2) in humans. *Science* 314, 1898–1903. doi:10.1126/science.1132745
- Kumar, S., Henrickson, K.J., 2012. Update on Influenza Diagnostics: Lessons from the Novel H1N1 Influenza A Pandemic. *Clin. Microbiol. Rev.* 25, 344–361. doi:10.1128/CMR.05016-11
- Lee, H.K., Tang, J.W.-T., Kong, D.H.-L., Koay, E.S.-C., 2013a. Simplified Large-Scale Sanger Genome Sequencing for Influenza A/H3N2 Virus. *PLoS ONE* 8. doi:10.1371/journal.pone.0064785
- Lee, H.K., Tang, J.W.-T., Kong, D.H.-L., Loh, T.P., Chiang, D.K.-L., Lam, T.T.-Y., Koay, E.S.-C., 2013b. Comparison of Mutation Patterns in Full-Genome A/H3N2 Influenza Sequences Obtained Directly from Clinical Samples and the Same Samples after a Single MDCK Passage. *PLoS ONE* 8, e79252. doi:10.1371/journal.pone.0079252
- Liechti, R., Gleizes, A., Kuznetsov, D., Bougueleret, L., Mercier, P.L., Bairoch, A., Xenarios, I., 2010. OpenFluDB, a database for human and animal influenza virus. *Database* 2010, baq004. doi:10.1093/database/baq004
- Lin, Y.P., Xiong, X., Wharton, S.A., Martin, S.R., Coombs, P.J., Vachieri, S.G., Christodoulou, E., Walker, P.A., Liu, J., Skehel, J.J., Gamblin, S.J., Hay, A.J., Daniels, R.S., McCauley, J.W., 2012. Evolution of the receptor binding properties of the influenza A(H3N2) hemagglutinin. *Proc. Natl. Acad. Sci.* 109, 21474–21479. doi:10.1073/pnas.1218841110
- Łuksza, M., Lässig, M., 2014. A predictive fitness model for influenza. *Nature* 507, 57–61. doi:10.1038/nature13087
- Matrosovich, M., Matrosovich, T., Carr, J., Roberts, N.A., Klenk, H.-D., 2003. Overexpression of the alpha-2,6-sialyltransferase in MDCK cells increases influenza virus sensitivity to neuraminidase inhibitors. *J. Virol.* 77, 8418–8425.
- Meyer, A.G., Wilke, C.O., 2015. Geometric Constraints Dominate the Antigenic Evolution of Influenza H3N2 Hemagglutinin. *PLoS Pathog.* 11. doi:10.1371/journal.ppat.1004940
- Meyer, A.G., Wilke, C.O., 2013. Integrating Sequence Variation and Protein Structure to Identify Sites under Selection. *Mol. Biol. Evol.* 30, 36–44. doi:10.1093/molbev/mss217
- Neher, R.A., Bedford, T., 2015. nextflu: real-time tracking of seasonal influenza virus evolution in humans. *Bioinformatics* 31. doi:10.1093/bioinformatics/btv381
- Neher, R.A., Russell, C.A., Shraiman, B.I., 2014. Predicting evolution from the shape of genealogical trees. *eLife* 3, e03568. doi:10.7554/eLife.03568
- Nelson, M.I., Simonsen, L., Viboud, C., Miller, M.A., Taylor, J., George, K.S., Griesemer, S.B., Ghedin, E., Sengamalai, N.A., Spiro, D.J., Volkov, I., Grenfell, B.T., Lipman, D.J., Taubenberger, J.K., Holmes, E.C., 2006. Stochastic Processes Are Key Determinants of Short-Term Evolution in Influenza A Virus. *PLoS Pathog* 2, e125. doi:10.1371/journal.ppat.0020125

- Oh, D.Y., Barr, I.G., Mosse, J.A., Laurie, K.L., 2008. MDCK-SIAT1 cells show improved isolation rates for recent human influenza viruses compared to conventional MDCK cells. *J. Clin. Microbiol.* 46, 2189–2194. doi:10.1128/JCM.00398-08
- Pan, K., Deem, M.W., 2011. Quantifying selection and diversity in viruses by entropy methods, with application to the haemagglutinin of H3N2 influenza. *J. R. Soc. Interface* 8, 1644–1653. doi:10.1098/rsif.2011.0105
- Pond, S.L.K., Frost, S.D.W., Muse, S.V., 2005. HyPhy: hypothesis testing using phylogenies. *Bioinformatics* 21, 676–679. doi:10.1093/bioinformatics/bti079
- Price, M.N., Dehal, P.S., Arkin, A.P., 2010. FastTree 2 – Approximately Maximum-Likelihood Trees for Large Alignments. *PLoS ONE* 5, e9490. doi:10.1371/journal.pone.0009490
- Robertson, J.S., Nicolson, C., Major, D., Robertson, E.W., Wood, J.M., 1993. The role of amniotic passage in the egg-adaptation of human influenza virus is revealed by haemagglutinin sequence analyses. *J. Gen. Virol.* 74 ( Pt 10), 2047–2051. doi:10.1099/0022-1317-74-10-2047
- Shih, A.C.-C., Hsiao, T.-C., Ho, M.-S., Li, W.-H., 2007. Simultaneous amino acid substitutions at antigenic sites drive influenza A hemagglutinin evolution. *Proc. Natl. Acad. Sci.* 104, 6283–6288. doi:10.1073/pnas.0701396104
- Skowronski, D.M., Janjua, N.Z., De Serres, G., Sabaiduc, S., Eshaghi, A., Dickinson, J.A., Fonseca, K., Winter, A.-L., Gubbay, J.B., Krajden, M., Petric, M., Charest, H., Bastien, N., Kwindt, T.L., Mahmud, S.M., Van Caesele, P., Li, Y., 2014. Low 2012–13 Influenza Vaccine Effectiveness Associated with Mutation in the Egg-Adapted H3N2 Vaccine Strain Not Antigenic Drift in Circulating Viruses. *PLoS ONE* 9, e92153. doi:10.1371/journal.pone.0092153
- Spielman, S., Wan, S., Wilke, C.O., 2015. One-rate models outperform two-rate models in site-specific dN/dS estimation. *bioRxiv* 032805. doi:10.1101/032805
- Squires, R.B., Noronha, J., Hunt, V., García-Sastre, A., Macken, C., Baumgarth, N., Suarez, D., Pickett, B.E., Zhang, Y., Larsen, C.N., Ramsey, A., Zhou, L., Zaremba, S., Kumar, S., Deitrich, J., Klem, E., Scheuermann, R.H., 2012. Influenza Research Database: an integrated bioinformatics resource for influenza research and surveillance. *Influenza Other Respir. Viruses* 6, 404–416. doi:10.1111/j.1750-2659.2011.00331.x
- Stöhr, K., Bucher, D., Colgate, T., Wood, J., 2012. Influenza Virus Surveillance, Vaccine Strain Selection, and Manufacture, in: Kawaoka, Y., Neumann, G. (Eds.), *Influenza Virus, Methods in Molecular Biology*. Humana Press, pp. 147–162.
- Suzuki, Y., 2008. Positive selection operates continuously on hemagglutinin during evolution of H3N2 human influenza A virus. *Gene* 427, 111–116. doi:10.1016/j.gene.2008.09.012
- Suzuki, Y., 2006. Natural selection on the influenza virus genome. *Mol. Biol. Evol.* 23, 1902–1911. doi:10.1093/molbev/msl050
- The World Health Organization, 2015. Recommended composition of influenza virus vaccines for use in the 2015- 2016 northern hemisphere influenza season.
- Tien, M.Z., Meyer, A.G., Sydykova, D.K., Spielman, S.J., Wilke, C.O., 2013. Maximum allowed solvent accessibilities of residues in proteins. *PLoS One* 8, e80635. doi:10.1371/journal.pone.0080635
- Tusche, C., Steinbrück, L., McHardy, A.C., 2012. Detecting patches of protein sites of influenza A viruses under positive selection. *Mol. Biol. Evol.* 29, 2063–2071. doi:10.1093/molbev/mss095
- WHO Writing Group, Ampofo, W.K., Baylor, N., Cobey, S., Cox, N.J., Daves, S., Edwards, S., Ferguson, N., Grohmann, G., Hay, A., Katz, J., Kullabutr, K., Lambert, L., Levandowski, R., Mishra, A.C., Monto, A., Siqueira, M., Tashiro, M., Waddell, A.L., Wairagkar, N., Wood, J., Zambon, M., Zhang, W., 2012. Improving influenza vaccine virus selectionReport of a WHO informal consultation held at WHO headquarters, Geneva,

- Switzerland, 14–16 June 2010. *Influenza Other Respir. Viruses* 6, 142–152.  
doi:10.1111/j.1750-2659.2011.00277.x
- Wickham, H., 2009. *ggplot2: elegant graphics for data analysis*. Springer New York.
- Wolf, Y.I., Viboud, C., Holmes, E.C., Koonin, E.V., Lipman, D.J., 2006. Long intervals of stasis punctuated by bursts of positive selection in the seasonal evolution of influenza A virus. *Biol. Direct* 1, 34. doi:10.1186/1745-6150-1-34
- World Health Organization Global influenza surveillance network, 2011. *Manual for the laboratory diagnosis and virological surveillance of influenza*. Geneva, Switzerland.
- Wyde, P.R., Couch, R.B., Mackler, B.F., Cate, T.R., Levy, B.M., 1977. Effects of Low- and High-Passage Influenza Virus Infection in Normal and Nude Mice. *Infect. Immun.* 15, 221–229.
- Xie, H., Wan, X.-F., Ye, Z., Plant, E.P., Zhao, Y., Xu, Y., Li, X., Finch, C., Zhao, N., Kawano, T., Zoueva, O., Chiang, M.-J., Jing, X., Lin, Z., Zhang, A., Zhu, Y., 2015. H3N2 Mismatch of 2014–15 Northern Hemisphere Influenza Vaccines and Head-to-head Comparison between Human and Ferret Antisera derived Antigenic Maps. *Sci. Rep.* 5. doi:10.1038/srep15279

**Figure 1. Schematic of influenza A virus sequence collection and analysis.** (A) Typical processing steps of influenza A virus clinical isolates. Virus collected from patients may be passaged serially prior to PCR amplification and sequencing in a variety of different environments (Ex. canine cell culture, monkey cell culture, egg amniotes). However, some clinical virus is not passaged and is sequenced directly. (B) Phylogenetic tree of H3N2 HA sequences from the 2005-2015 seasons. The inset shows a small clade of sequences from the 2006/2007 season, with colored dots representing sequences with passage annotations (red virion: unpassaged, blue dog: canine cell culture, gray hen: egg amniote, unlabeled: missing passage history annotation).

**Figure 2. Comparison of sitewise  $dN/dS$  values among sequences with differing passage histories.** (A–C) Pearson correlations between sitewise  $dN/dS$  values for HA sequences derived from passaged and unpassaged influenza virus collected between 2005 and 2015 (downsampled to  $n = 917$  in all groups). Correlations were calculated separately for  $dN/dS$  estimated from complete trees (A), internal branches only (B), and tip branches only (C). Asterisks denote significance of correlations ( $*0.01 \leq P < 0.05$ ,  $**0.001 \leq P < 0.01$ ,  $***P < 0.001$ ). (D) Scatter plots show the raw sitewise  $dN/dS$  values used to calculate the correlations in parts A–C. We tested for systematic differences in  $dN/dS$  values with paired  $t$  tests, and significant differences are indicated with asterisks ( $*0.01 \leq P < 0.05$ ,  $**0.001 \leq P < 0.01$ ,  $***P < 0.001$ ). Data used to generate this figure are available in Supplementary Dataset 1.

**Figure 3. Percent variance in  $dN/dS$  explained by relative solvent accessibility (A) and by inverse distance to protein site 224 (B).** (A) Relative solvent accessibility (RSA) explains ~10%–16% of the variation in  $dN/dS$  for all sequences. (B) Inverse distance to site 224 explains ~7% of the variation in  $dN/dS$  for cell-passaged sequences and for all sequences (pooled), however it explains virtually no variation for unpassaged sequences. Asterisks denote significance of correlations ( $*0.01 \leq P < 0.05$ ,  $**0.001 \leq P < 0.01$ ,  $***P < 0.001$ ). Data used to generate this figure are available in Supplementary Dataset 1.

**Figure 4. Virus passaged in non-SIAT1 cells carries unique adaptations not present in unpassaged or SIAT1-passaged virus.** For size matched groups of sequences collected between 2005 and 2015 ( $n = 1046$ ), (A) the correlation between  $dN/dS$  and RSA is weakened for virus passaged in non-SIAT1 cells. (B) The correlation between  $dN/dS$  and inverse distance to site 224, representing a positive-selection hotspot in the vicinity of that site, is only present in virus passaged in non-SIAT1 cells. (C) Scatter plots show individual  $dN/dS$  values obtained from the full phylogenetic tree, internal branches only, and tip branches only. For the full tree, internal branches, and tip branches,  $dN/dS$  in non-SIAT1-passaged virus is significantly elevated relative to unpassaged and SIAT1-passaged virus (paired  $t$  test). Asterisks denote significance



levels ( $*0.01 \leq P < 0.05$ ,  $**0.001 \leq P < 0.01$ ,  $***P < 0.001$ ). Data used to generate this figure are available in Supplementary Dataset 3.

**Figure 5. Correlations mapped onto the hemagglutinin structure for non-SIAT1-passaged and unpassaged sequences.** The correlation between  $dN/dS$  and inverse distance for each reference site was mapped onto the hemagglutinin structure for (A) non-SIAT1 sequences and (B) unpassaged sequences collected between 2005 and 2015 ( $n = 1703$ ). Red coloring represents positive correlations, while white represents zero or negative correlations. Non-SIAT1-passaged and unpassaged sequences yield distinct correlation patterns. In particular, the loop containing site 224 lights up strongly for non-SIAT1-passaged sequences but not for unpassaged sequences. Data used to generate this figure are available in Supplementary Dataset 5.

**Figure 6. Unpassaged sequences allow recovery of antigenic regions from positive-selection analysis.** For each site, the correlation between  $dN/dS$  and inverse distance (A) or  $dN/dS$  directly (B) were mapped onto the hemagglutinin structure, for  $dN/dS$  derived from unpassaged sequences collected between 2005 and 2015 ( $n = 1703$ ). Red coloring represents higher correlation; blue coloring represents higher  $dN/dS$ . Highlighted regions contain sites (labeled with protein site number) which experimentally determined to be antigenic by (Koel et al., 2013) and sites experimentally determined by (Chambers et al., 2015) to be responsible for antigenic escape of the 2014-2015 influenza. Correlations and  $dN/dS$  for antigenic sites are given in Table 2. Data used to generate this figure are available in Supplementary Dataset 5.

**Supplementary Figure 1. Comparison of sitewise hemagglutinin  $dN/dS$  derived from size-matched samples of sequences with various passage histories, including egg amniotes.** Pearson correlations between sitewise  $dN/dS$  values for HA sequences derived from passaged and unpassaged influenza virus collected between 2005 and 2015, randomly down-sampled to 79 sequences per passage group. (Since there were so few egg-derived sequences, each down-sampling was independently performed three times, resulting in replicates 1, 2, and 3 for each passage group.) Correlations were calculated separately for complete trees (A), internal branches only (B), and tip branches only (C). Asterisks denote significance of correlations ( $*0.01 \leq P < 0.05$ ,  $**0.001 \leq P < 0.01$ ,  $***P < 0.001$ ). Data used to generate this figure are available in Supplementary Dataset 2.

**Supplementary Figure 2. Comparison of unpassaged, non-SIAT1-passaged, and SIAT1-passaged virus in 2014 only.** (A–C) Pearson correlations between sitewise  $dN/dS$  values for the three passage groups ( $n = 249$ ), for complete trees, internal branches only, and tip branches only, respectively. (D) Scatter plots show the raw sitewise  $dN/dS$  values used to calculate the correlations in parts A–C. We tested for



systematic differences in  $dN/dS$  values with paired  $t$  tests, and significant differences are indicated with asterisks ( $*0.01 \leq P < 0.05$ ,  $**0.001 \leq P < 0.01$ ,  $***P < 0.001$ ). For the full tree,  $dN/dS$  in both non-SIAT1-passaged virus and SIAT1-passaged virus is significantly elevated relative to unpassaged virus. For tip branches,  $dN/dS$  in non-SIAT1-passaged virus is significantly elevated relative to unpassaged virus. No significant difference was found for internal branches. Data used to generate this figure are available in Supplementary Dataset 4.

**Supplementary File 1.** GISAID acknowledgements for hemagglutinin sequences collected between 1968 and 2015.

**Supplementary Dataset 1.** Data used to generate Figures 2 and 3. This file includes 1) sitewise  $dN/dS$  values of random draws of 917 unpassaged, generic cell cultured, monkey cell cultured, and the pooled group sequences collected between 2005 and 2015, 2) protein and gene numbering, 3) PDB:2YP7 sequence, 4) relative solvent accessibilities of the hemagglutinin trimer, and 5) linear distances to protein site 224.

**Supplementary Dataset 2.** Data used to generate Supplementary Figure 1. This file includes 1) sitewise  $dN/dS$  values of random draws of 97 unpassaged, generic cell cultured, egg cultured, monkey cell cultured, and the pooled group sequences collected between 2005 and 2015, 2) protein and gene numbering, 3) PDB:2YP7 sequence.

**Supplementary Dataset 3.** Data used to generate Figure 4. This file includes 1) sitewise  $dN/dS$  values of random draws of 1046 unpassaged, SIAT1, and non-SIAT1 cell culture sequences collected between 2005 and 2015, 2) protein and gene numbering, 3) PDB:2YP7 sequence, 4) relative solvent accessibilities of the hemagglutinin trimer, and 5) linear distances to protein site 224.

**Supplementary Dataset 4.** Data used to generate Supplementary Figure 2. This file includes 1) sitewise  $dN/dS$  values of random draws of 249 unpassaged, SIAT1 cultured, and non-SIAT1 cell cultured sequences collected in 2014, 2) protein and gene numbering, 3) PDB:2YP7 sequence.

**Supplementary Dataset 5.** Data used to generate Figures 5 and 6. This file includes 1) sitewise  $dN/dS$  values of random draws of 1703 unpassaged and non-SIAT1 cell cultured sequences collected between 2005 and 2015, 2) protein and gene numbering, 3) PDB:2YP7 sequence, 4) sitewise inverse distance correlations.

**Supplementary Dataset 6.** This file includes 1) all sitewise  $dN/dS$  values used to generate figures, 2) protein and gene numbering, 3) PDB:2YP7 sequence, 4) relative solvent accessibilities of the hemagglutinin trimer, and 5) linear distances to protein site 224.

**Table 1. Parsing of passage-annotated FASTA sequences into passage history groups.** For each passage group, we defined a regular expression that could reliably identify sequences with that passage history. Regular expressions were applied through the built-in python library “re”. The right three columns list the number of sequences we identified for each passage group, for years 2005–2015, 2014 only, and 2015 only.

Passage group	Regular expression	Number of sequences		
		2005–2015	2014	2015
Chicken egg amniotes	AM[1-9] E[1-7] AMNIOTIC EGG EX AM_[1-9]	79	6	0
Monkey cell culture	TMK RMK RHMK R  PMK R[1-9] RX	917	366	290
Generic cell culture	S[1-9] SX SIAT MDCK C[1-9] CX C_[1-9] M[1-9] MX X[1-9] ^X_\$	3041	794	787
SIAT1	^S[1-9]_\$ ^SX_\$ SIAT2_SIAT1 SIAT3_SIAT1	1046	389	626
Non-SIAT1 cell culture	not SIAT SX S[1-9]	1755	297	56
Unpassaged	LUNG P0 OR_ ORIGINAL CLINICAL DIRECT	1703	249	506

**Table 2. Evolutionary rates and inverse distance correlations of antigenic sites.**

For each site, we determined  $dN/dS$  and the correlation between  $dN/dS$  and inverse distance for unpassaged sequences collected between 2005 and 2015 ( $n = 1703$ ). 7/8 antigenic sites have inverse-distance correlations above the 90<sup>th</sup> percentile, while only 2/8 antigenic sites have  $dN/dS$  values above the 90<sup>th</sup> percentile. Antigenic sites were experimentally determined by (Chambers et al., 2015) and (Koel et al., 2013).

Antigenic site			Raw $dN/dS$		Inv.-dist. correlation	
Gene	Protein	Study	$dN/dS$	percentile	$r$	percentile
161	145	Koel	1.828	0.863	0.071	0.910
171	155	Koel	0	0.002	0.061	0.871
172	156	Koel	1.371	0.805	0.116	0.982
174	158	Koel	3.244	0.965	0.157	0.994
175	159	Koel, Chambers	0.936	0.738	0.165	0.998
176	160	Chambers	2.922	0.953	0.133	0.980
205	189	Koel	0.965	0.748	0.076	0.928
209	193	Koel	1.829	0.879	0.084	0.947

**Figure 1**

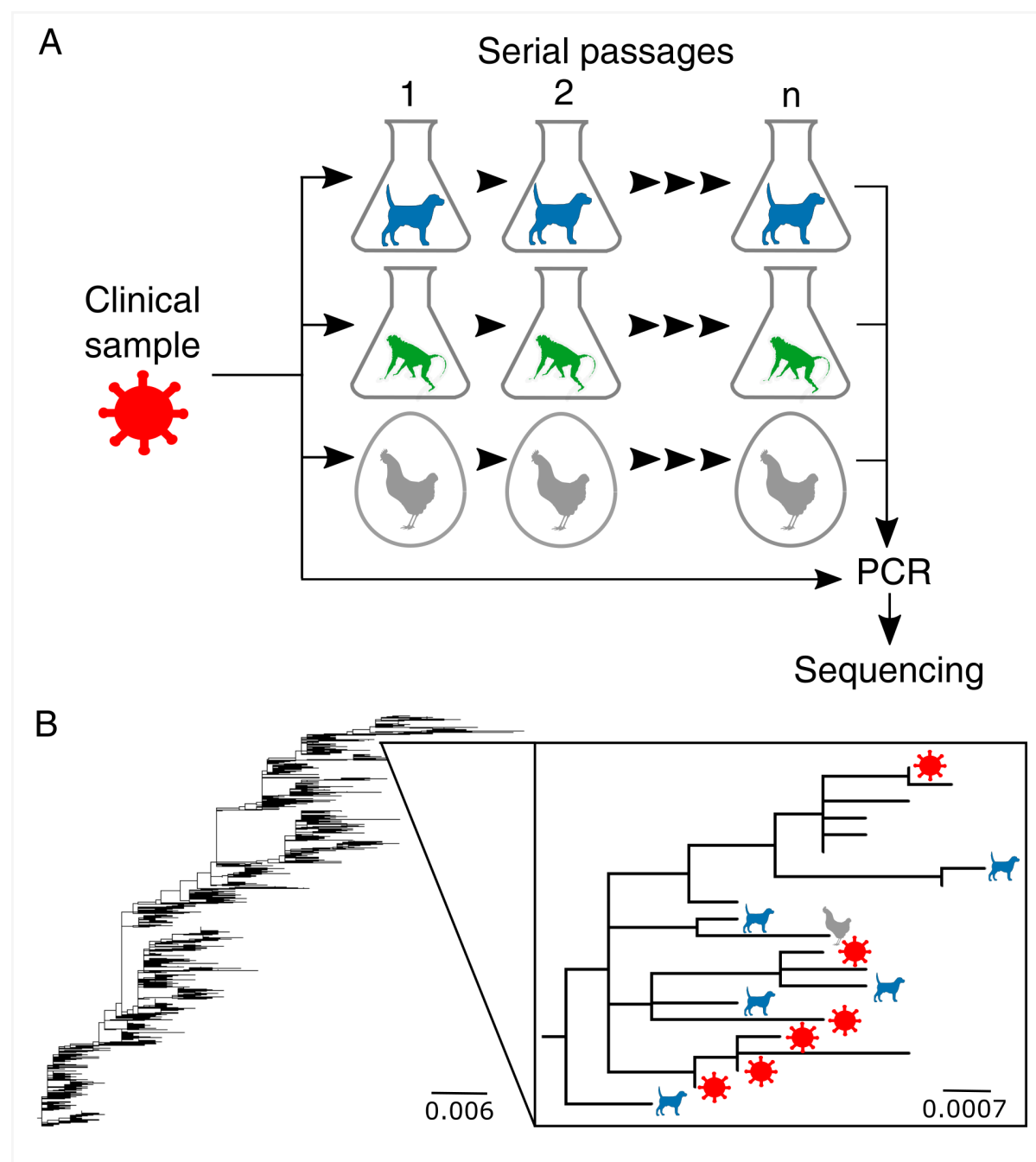
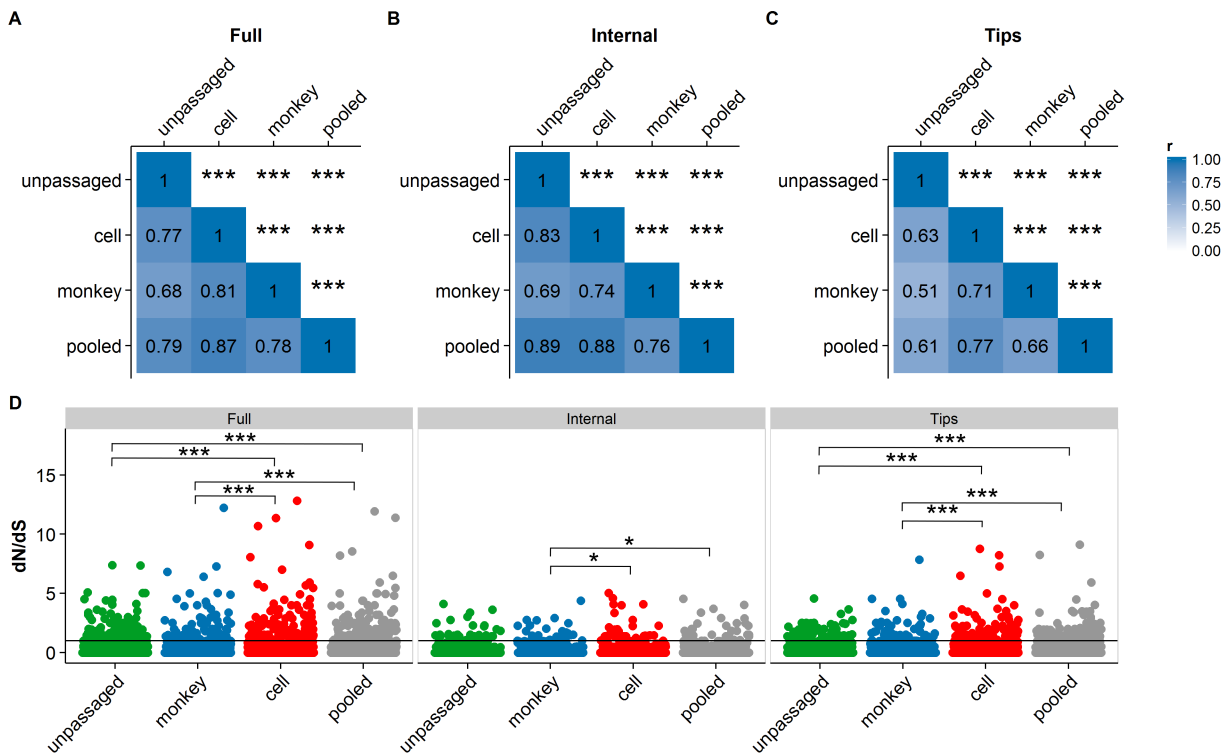
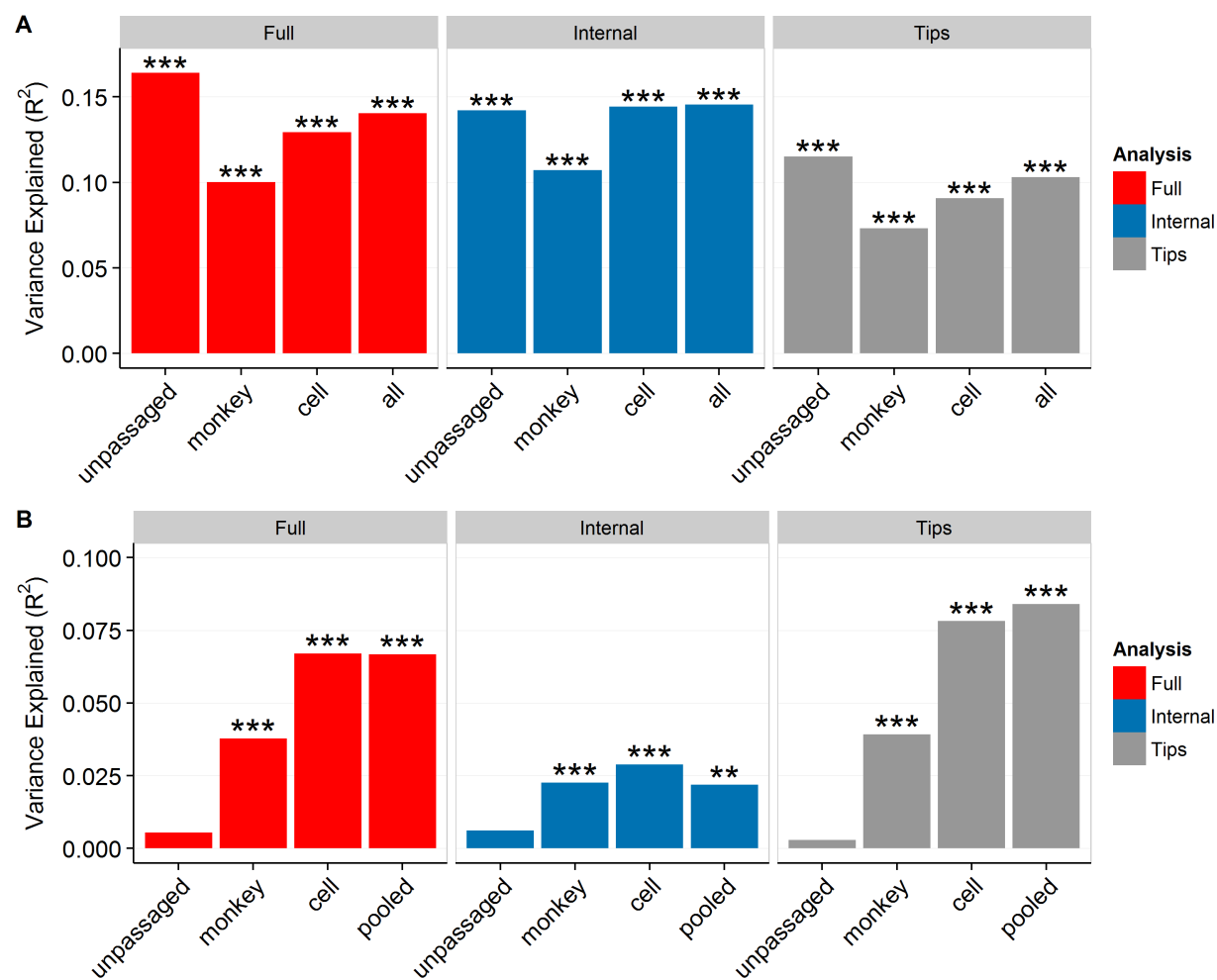


Figure 2



**Figure 3**





**Figure 4**

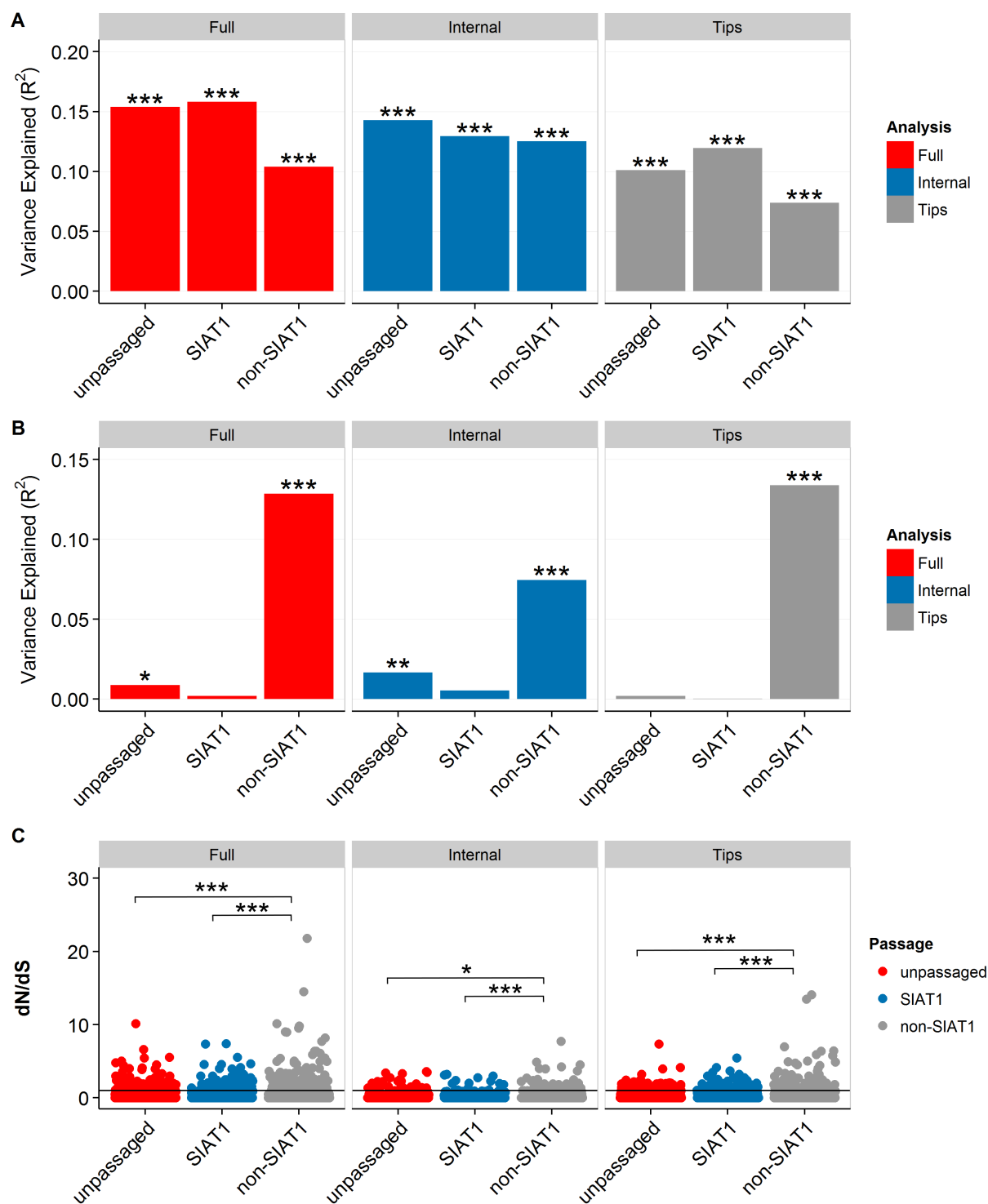


**Figure 5**

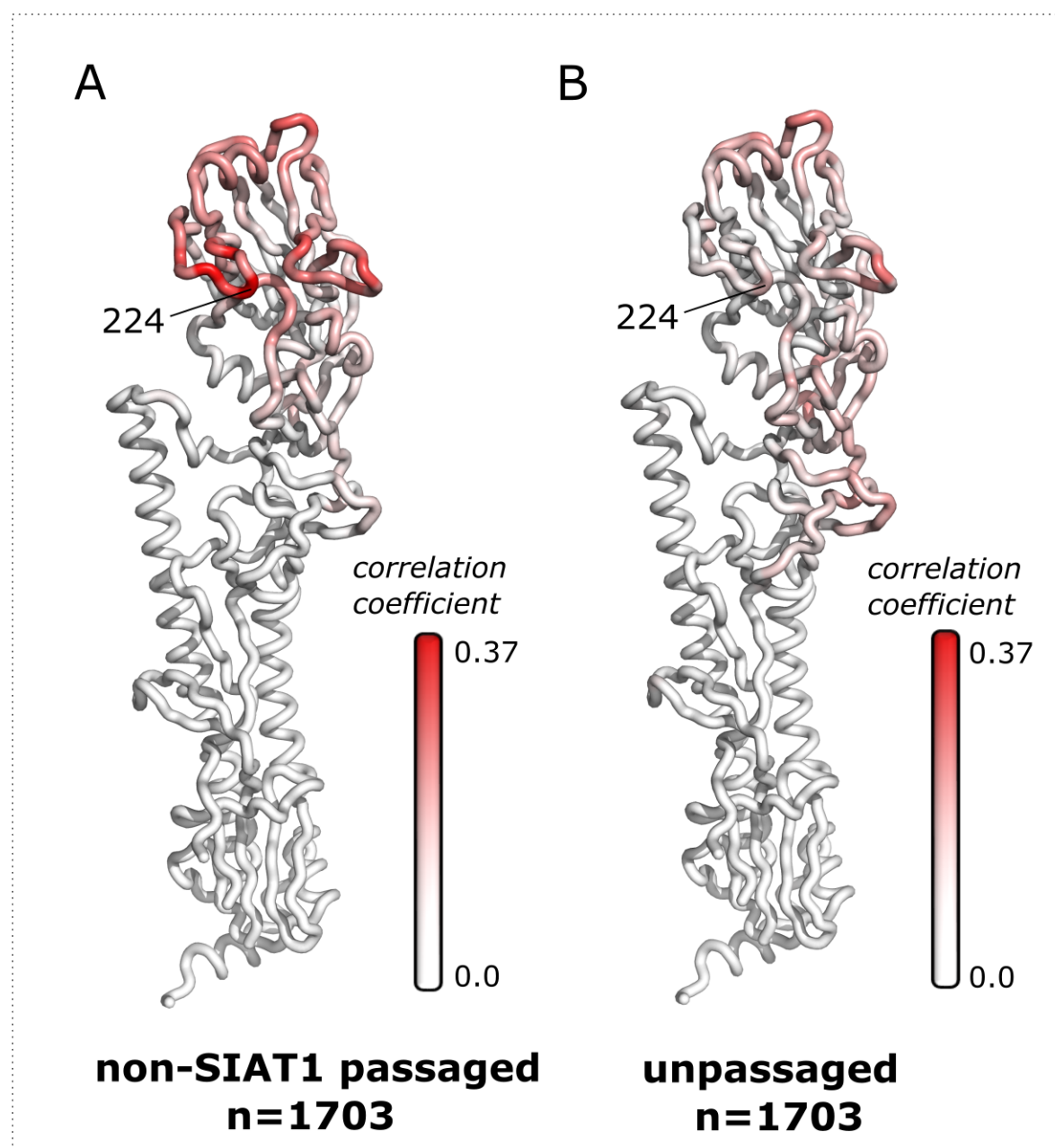


**Figure 6**

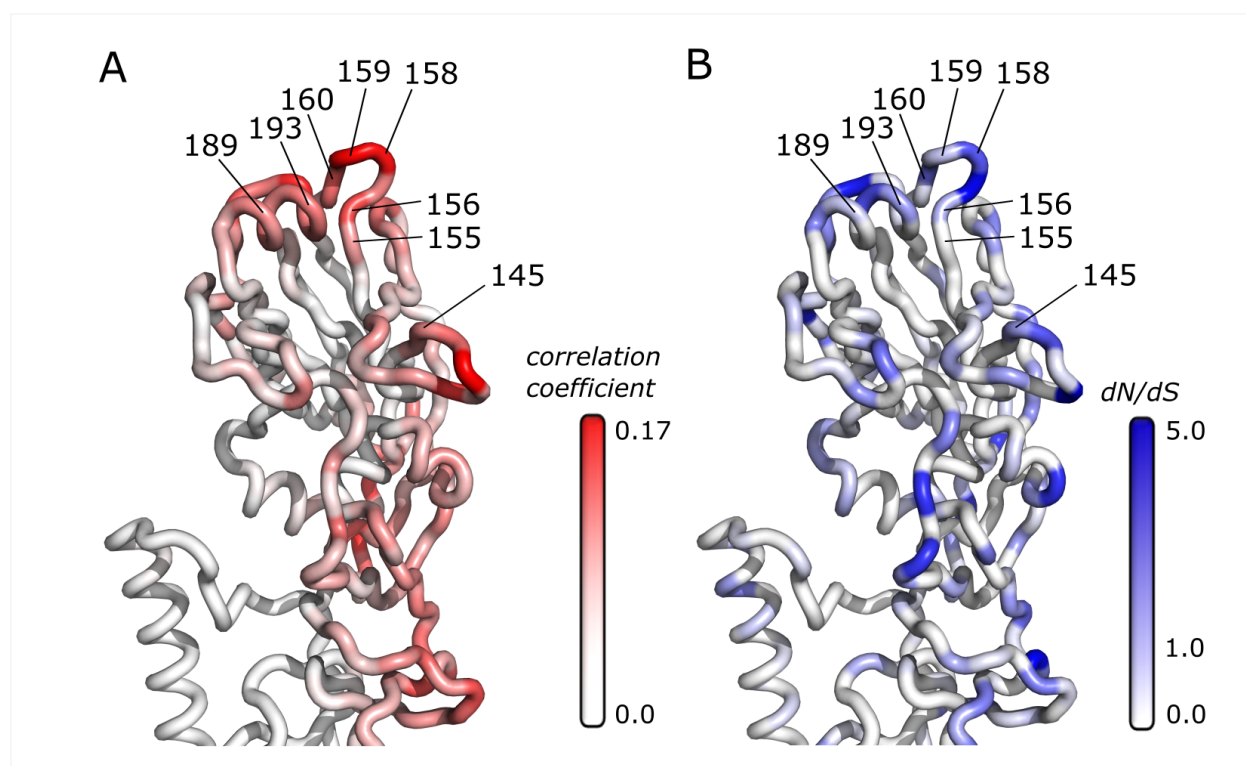


**Figure S1**

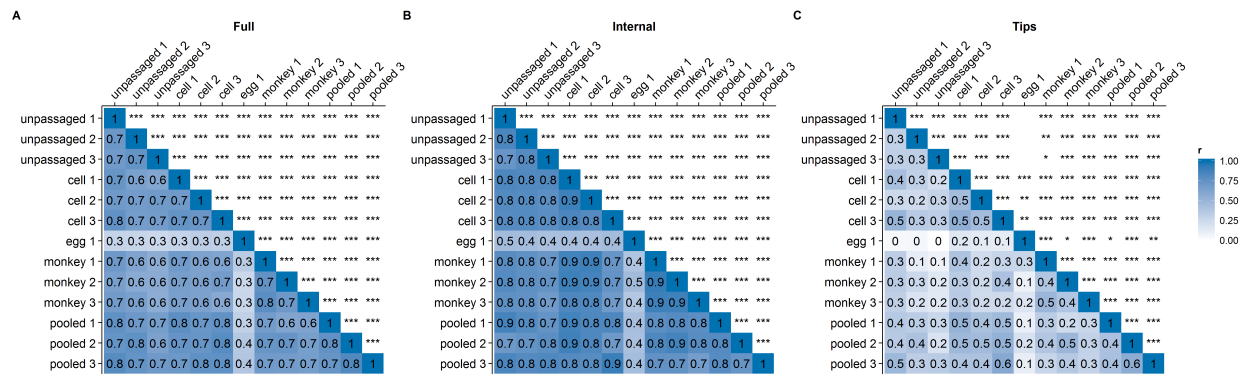


**Figure S2**

